# *Irx3* Promotes Gap Junction Communication Between Uterine Stromal Cells to Regulate Vascularization during Embryo Implantation

Ryan M. Brown[1], Linda Wang[1], Anqi Fu[1], Athilakshmi Kannan[2], Michael Mussar[1], Indrani C. Bagchi[2*], Joan S. Jorgensen[1*]

1. Department of Comparative Biosciences, University of Wisconsin-Madison, Madison, WI, United States of America
2. Department of Comparative Biosciences, University of Illinois at Urbana Champaign, Urbana, IL, United States of America

*Co-corresponding authors: Indrani Bagchi and Joan S. Jorgensen

Email address: ibagchi@illinois.edu; joan.jorgensen@wisc.edu

Short title: *Irx3* promotes successful embryo-uterine interactions in mice

**Funding**

National Institutes of Health, Eunice Kennedy Shriver National Institute Of Child Health & Human Development (NIH-NICHD) R01HD075079 (JSJ)

National Institutes of Health, Eunice Kennedy Shriver National Institute Of Child Health & Human Development (NIH-NICHD) R01HD090066 (IB)

Endocrinology and Reproductive Physiology Training Grant, and National Institutes of Health (NIH-NICHD) T32HD41921 (AF).

**Abstract**

Spontaneous abortions have been reported to affect up to 43% of parous women, with over 20% occurring before pregnancy is clinically diagnosed. Establishment of pregnancy is critically dependent on proper embryo-uterine interactions at the time of implantation. Besides oocyte abnormalities, implantation failure is a major contributor to early pregnancy loss. Previously, we demonstrated that two members of the Iroquois homeobox transcription factor family, IRX3 and IRX5, exhibited distinct and dynamic expression profiles in the developing ovary to promote oocyte and follicle survival. Elimination of each gene independently caused subfertility, but with different breeding pattern outcomes. *Irx3* KO ($Irx3^{LacZ/LacZ}$) females produced fewer pups throughout their reproductive lifespan which could only be partially explained by poor oocyte quality. Thus, we hypothesized that IRX3 is also expressed in the uterus where it acts to establish functional embryo-uterine interactions to support pregnancy. To test this hypothesis, we harvested pregnant uteri from control and *Irx3* KO females to evaluate IRX3 expression profiles and the integrity of embryo implantation sites. Our results indicate that IRX3 is expressed in the endometrial stromal cells of the pregnant uterus. Notably, of the days evaluated, IRX3 expression expanded into the endometrial stroma starting at day 4 of pregnancy (D4) with peak expression at D5-6, and then greatly diminished by D7. This pattern corresponds to the critical window for implantation and remodeling of the vasculature network in mice. Further, histology and immunohistochemistry at D7 showed that while embryos were able to attach to the uterus, implantation sites in *Irx3* KO pregnant mice exhibited impaired vascularization. In addition, our results showed significantly diminished expression of decidualization markers and disruptions in GJA1 organization in the decidual bed. These data, taken together with previous reports focused on the ovary, suggest that IRX3 promotes fertility via at least two different mechanisms: 1) promoting competent oocytes and 2) facilitating functional embryo-uterine interactions during implantation. Future research aims to tease apart

the roles for IRX3 in the oocyte versus the uterus and the mechanisms by which it promotes early embryo survival and a successful pregnancy outcome.

## Introduction

Embryo implantation is achieved when a competent oocyte is fertilized and then develops into a blastocyst capable of facilitating embryo-uterine interactions with the receptive endometrium. In humans, it has been reported that approximately two thirds of pregnancies are lost due to implantation failure. Uncovering the signaling pathways and downstream mediators that govern implantation are necessary to improve outcomes associated with defective embryo implantation including ectopic pregnancies, implantation failure and infertility (reviewed in [1]).

In the mammalian uterus, steroid hormones estrogen and progesterone induce structural and functional changes during early pregnancy to support embryo implantation [2-5]. Of these changes, uterine stromal differentiation, or decidualization, is a critical response to embryo recognition that initiates extensive tissue remodeling for proper maternal-fetal interactions during early pregnancy. During decidualization, the endometrial stromal cells of the uterus undergo differentiation into decidual cells with unique biosynthetic and secretory profiles needed to promote tissue transformation and uterine vascular remodeling [6-8]. In the murine model, implantation begins on day (D)4 midnight, with the majority of decidualization occurring between D5-8, and establishment of pregnancy by D10-11 of gestation [9]. Complementary timing occurs in the human uterus where, for a short window of time, during the mid-secretory phase of each menstrual cycle, the uterus becomes “receptive” to embryo implantation and the decidualization process begins [10]. In both the mouse and human, decidualization promotes tissue remodeling and neovascularization, which are critical events for successful establishment of pregnancy. A major challenge is deciphering the signaling mechanisms governing successful maternal-fetal interactions during early pregnancy. To this end, it is necessary to identify and characterize factors that regulate decidualization and angiogenesis during embryo implantation.

The Iroquois factors are highly conserved proteins that have been implicated in patterning and embryogenesis in animal kingdoms spanning invertebrate to vertebrate. In mammals, there are a total of six Iroquois genes clustered in two groups, with cluster A (*Irx1,2,4*) and cluster B (*Irx3,5,6*) located on chromosomes 5 and 16 in the human and 8 and 13 in the mouse, respectively [11, 12]. Previously, we discovered that null mutation of both *Irx3* and *Irx5* resulted in abnormal granulosa cell morphology and disrupted granulosa cell-oocyte interactions [13]. A closer look, using $Irx3^{LacZ/LacZ}$ single knockout mice, revealed that although mutant females could become pregnant, loss of *Irx3* caused a decrease in birthrate to approximately half as many pups compared to controls throughout a 6-month breeding study. While $Irx3^{LacZ/LacZ}$ females demonstrated abnormalities in follicle survival, this did not fully explain the subfertility phenotype [13].

Although evidence points to an oocyte deficit with loss of *Irx3,* ovarian histology led us to hypothesize that another facet in the female reproductive axis could be disrupted. Due to the decrease in pup accumulation over time, we hypothesized that embryo implantation was compromised due to loss of *Irx3*. Evaluation of implantation sites within $Irx3^{LacZ/LacZ}$ pregnant females demonstrated impaired vascularization and a significant reduction in pups by D7 of pregnancy. Herein, we report for the first time that *Irx3* is expressed in the mouse uterus overlapping the window of implantation when it plays a critical role in neoangiogenesis. Our results suggest disruptions are caused by unorganized gap junction (GJA1) protein expression. Together, these findings reveal the multifaceted role of *Irx3* in female fertility.

## Materials and Methods

### Ethics Statement

Animals were euthanized by $CO_2$ asphyxiation followed by cervical dislocation. Animal housing and all described procedures were reviewed and approved by the Institutional Animal Care and Use Committee at the University of Wisconsin – Madison and were performed in

accordance with National Institute of Health Guiding Principles for the Care and Use of Laboratory Animals.

## Animals

Mice were housed in disposable, ventilated cages (Innovive, San Diego, CA). Rooms were maintained at 22 ± 2°C and 30–70% humidity on a 12-hour light/dark cycle. Mouse strains included CD1 outbred mice (Crl:CD1(ICR), Charles River, Wilmington, MA, USA) and *Irx3*$^{LacZ}$ [14], all of which were maintained on a CD1 genetic background. Genotyping was carried out as previously reported [13, 14]. Pregnancies were the result of breeding between CD1 (WT control) or *Irx3*$^{LacZ/LacZ}$ females and CD1 males. Thus, all embryos generated in *Irx3*$^{LacZ/LacZ}$ females were *Irx3*$^{+/LacZ}$. Timed mating was identified as the presence of a vaginal plug after mating which was designated as day 1 (D1) of pregnancy.

## Tissue Processing and Histology

Uterine tissue was harvested at the indicated timepoints, fixed in 10% neutral buffer formalin (NBF) in phosphate buffer saline (PBS) at 4°C overnight. Uteri were collected on D7 of gestation, dehydrated through an ethanol gradient, cleared in xylene and embedded in paraffin. Paraffin blocks were sectioned at 5μm thickness, mounted on slides and then stained with hematoxylin and eosin (H&E) for histological analysis.

## Immunohistochemistry/Immunofluorescence

Uterus tissue sections were deparaffinized in xylene, rehydrated through a series of ethanol washes, and then rinsed in water. Antigen retrieval was performed by immersing the slides in 0.1M citrate buffer solution at pH 6.0 or EDTA buffer at pH 8 depending on antibody specifications (Table S1), and heated in a water bath at 80°C for 25 min. The slides were

allowed to cool, rinsed in water, followed by PBS washes. Slides were then incubated at room temperature with 10% donkey solution for 1h before incubating them with primary antibody overnight at 4°C. The following morning, tissues were washed in PBS before incubating with secondary antibody for 1 hour, then washed with PBS, incubated with a 10X DAPI (4',6-diamidino-2-phenylindole) in PBS solution (1:500) as a nuclear counterstain for 10 minutes, followed by 3 minutes with Vector True View Kit (Vector Laboratories, SP-8400, Burlingame, CA), and mounted. Immunofluorescence was repeated in uterine sections collected from at least 3 animals. Quantification of IHC was performed using Image J, the mean fluorescence intensity of CD31 (n=3 for each group) or GJA1 (n = 3-4 for each group) were quantified using the ROI manager on both the mesometrial and anti-mesometrial regions surrounding the embryo. Images were collected on a Leica SP8 confocal microscope for IHC and a Keyence BZ-X700 microscope for H&E.

Quantitative real time PCR analysis (qPCR)

Uterine tissue was homogenized, and total RNA was extracted using TRIZOL reagent (Invitrogen, 15596026, Waltham, MA, USA), according to the manufacturer's protocol and quantified using a NanoDrop 2000. 500ng from each sample was used for First-Strand cDNA synthesis by SuperScriptII (Invitrogen, AM9515, Waltham, MA, USA). cDNA was diluted 1:5 and then 2μl was added to 5ul SYBR green PCR mixture (BioRad, 1725271, Hercules, CA, USA), 2.4ul water and 1.25 pmol primer mix. PCR reactions were carried out using the BioRad CFX96 system and RNA transcripts were quantified using the ΔΔCt method (Livak & Schmittgen, 2001). Primers, *36b4* 5' – CGACCTGGAAGTCCAACTAC – 3' R: 5' – ATCTGCTGCATCTGCTTG - 3' and *Irx3* F: 5' - CGCCTCAAGAAGGAGAACAAGA - 3', R: 5' - CGCTCGCTCCCATAAGCAT - 3' (IDT, Coralville, IA, USA)

151 Statistics

152 Statistics between groups were carried out using a two-sample t-test. Results were
153 considered statistically significant if p-values were ≤ 0.05.

154

155 **Results**

156 *Irx3*$^{LacZ/LacZ}$ females exhibit defects in uterine vascularization with a marked reduction in
157 implanted embryos

158 Previously, we determined that *Irx3*$^{LacZ/LacZ}$ females produced significantly fewer live pups
159 over time compared to their controls, resulting in a subfertility phenotype. Ovarian histology and
160 follicle counts identified oocyte deficits, but reproductive data suggested other factors were also
161 contributing to the subfertility phenotype [13]. To understand the impact of *Irx3* on female
162 fertility, we expanded our evaluation to examine uterine contributions of *Irx3* on fertility using
163 *Irx3*$^{LacZ/LacZ}$ mice and their littermate controls over time. We investigated the integrity of
164 implantation sites on D7 of pregnancy. Histological analysis of *Irx3*$^{LacZ/LacZ}$ (Fig 1B, D) and
165 control (Fig 1A, C) implantation sites at D7 of gestation demonstrate that loss of *Irx3* impairs
166 uterine vascularization, as depicted in the white boxes (Fig 1 A-D). To investigate whether
167 impaired implantation and defective vascularity were a result of hormonal deficiency, we
168 measured circulating estrogen and progesterone (Fig 1 E, F). Results showed that, estrogen
169 and progesterone levels were comparable between *Irx3*$^{LacZ/LacZ}$ and litter mate controls. To
170 assess when embryos were being lost in *Irx3*$^{LacZ/LacZ}$ females, we compared the number of
171 implanted embryos to that of control mice on D7 and D11 of gestation (Fig 1 G). By D7 we saw
172 a significant decrease in the number of pups *in utero* in the *Irx3*$^{LacZ/LacZ}$ mice; however, there was
173 no further reduction in pups between D7 and D11 indicating that pups were being lost during the
174 decidual phase of pregnancy. Together these data demonstrate that *Irx3* has a role in female
175 fertility with implications in uterine angiogenesis during embryo implantation.

176

177 *Irx3* expression is confined to a discrete window during embryo implantation.

178 Evidence of vascularity deficits within embryo implantation sites and early embryo loss
179 suggested a role for *Irx3* in uterine implantation. Thus, we examined the protein and transcript
180 profile of *Irx3* in the mouse uterus during normal pregnancy. Late on D4 of gestation, the mouse
181 uterus is receptive, and implantation ensues. At this time IRX3 protein expression is detected
182 predominately in the cytoplasm of the epithelial cells surrounding the lumen and uterine glands
183 (Fig 2A, B). By D5, which is the onset of endometrial stromal cell decidualization, IRX3 protein
184 expression is substantially increased, with expression expanding to the uterine stroma (S)
185 immediately surrounding the embryo (E), also referred to as the primary decidual zone (Fig 2 C,
186 D). Similarly, at D6 of gestation, IRX3 expression is prominently expressed throughout the
187 decidualized stroma, expanding further into the secondary decidual zone (Fig 2 E, F). On D7 of
188 gestation, nearing the end of the decidualization process, IRX3 protein expression is diminished
189 (Fig 2 G, H). Analysis of *Irx3* transcripts demonstrate a complimentary profile with expression
190 initially documented at D4, followed by substantial increases at the onset of decidualization at
191 D5 and D6 and a sharp decline toward the end of decidualization on D7. These data
192 demonstrate that *Irx3* is induced in endometrial stromal cells at the onset of embryo
193 implantation, the expression peaks during decidualization, and declines with the cessation of
194 decidual phase of pregnancy.
195
196 Endometrial stromal cell differentiation is impaired in $Irx3^{LacZ/LacZ}$ females
197 The close spatio-temporal relationship between *Irx3* expression and the progression of
198 decidualization led us to hypothesize that *Irx3* may play a role in this process. We, therefore,
199 evaluated the expression of known regulators of decidualization in $Irx3^{LacZ/LacZ}$ and control uteri.
200 Implantation sites were harvested at D7 and processed for RNA isolation and
201 immunofluorescence. Results show that as expected, *Irx3* expression was already low in WT
202 uteri at D7 (set to 1) and detectable, but extremely low (75-80% decreased) in the mutant

decidua. Any transcripts present were likely derived from embryo tissue contamination. While steroid receptor genes, *Esr1* and *Pgr1* remained unchanged, all other decidual markers were significantly decreased in mutant versus wild type implantation sites (Fig 3A). Further, HAND2 expression was weak in *Irx3*$^{LacZ/LacZ}$ D7 stroma compared to wild type as indicated by immunofluorescent analysis (Fig 3B), supporting qPCR results and suggesting defective decidualization.

Compromised neoangiogenesis in the decidual bed of *Irx3* KO females

To further evaluate the vascularization defect found in *Irx3*$^{LacZ/LacZ}$ implantation sites, we examined whether loss of *Irx3* expression affected angiogenesis. Thus, we analyzed the angiogenic response in *Irx3*$^{LacZ/LacZ}$ uteri by monitoring an endothelial cell marker, CD31 (platelet endothelial cell adhesion molecule-1, PECAM-1), at D7 of gestation (Fig 4 A-G). As expected, implantation sites from control mice exhibited prominent CD31 expression in both the antimesometrial (AM) and mesometrial (M) areas on day 7 of pregnancy (Fig 4 A, C, E). In contrast, while expression of CD31 in *Irx3*$^{LacZ/LacZ}$ implantation sites was not different in the mesometrial side (Fig 4D, G), quantification of expression showed a significant decrease of CD31 expression in the antimesometrial region (Fig 4B, F, G). The decrease in the level of CD31 at the implantation site of *Irx3*$^{LacZ/LacZ}$ uteri on D7 raises the possibility that *Irx3* is mediating embryo-uterine interactions through promotion of a robust angiogenic response during implantation.

Fewer and unorganized gap junction connections in *Irx3*$^{LacZ/LacZ}$ uteri

To gain insights on the impact of *Irx3* loss on decidualization and vascularization, we investigated GJA1, a gap junction protein critical in modulating stromal differentiation and neovascularization during murine implantation [15]. In our previous investigations, *Irx3*$^{LacZ/LacZ}$ ovaries demonstrated no change in *Gja1* transcripts between mutant and control, but they

229 detected abnormal deposition of GJA1, which resulted in follicle death [13]. Based on these
230 data, we tested whether loss of *Irx3* in the uterus would impair GJA1 expression during embryo
231 implantation. Complementary to our ovarian expression data, we found that loss of *Irx3* resulted
232 in no change in Gja1 transcripts (Fig 5A), but significantly disrupted GJA1 protein localization in
233 both mesometrial and anti-mesometrial regions of the uterine stroma (Fig 5 B-J). Together these
234 data suggest that *Irx3* functions to promote embryo implantation through appropriate cell-cell
235 communication to provide the proper environment for successful decidualization and
236 neovascularization.
237
238 **Discussion**
239 The Iroquois genes have been implicated in embryonic patterning and can be found in a
240 range of tissues, with roles in organization of the spinal cord, limb, bone and heart, to name a
241 few [12, 16-18]. Previously, we identified IRX3 and IRX5 expression in mouse ovaries, but not
242 testis, starting after sex determination [19]. This led to a series of investigations to discern the
243 role of IRX3 and IRX5 in the ovary during development. Using mutant mice lacking both *Irx3*
244 and *Irx5*, we discovered mutant ovaries had abnormal granulosa cell morphology and disturbed
245 granulosa cell-oocyte interactions [13]. A closer look at ablation of *Irx3* alone, using $Irx3^{LacZ/LacZ}$
246 mutant females, indicated that loss of *Irx3* caused reduced follicle numbers; however, this did
247 not fully explain the profound deficit in fertility as indicated by at least 50% loss in live pup births
248 compared to wild type females [20]. This prompted us to investigate whether IRX3 was affecting
249 embryo implantation. Results from the current study suggest multifaceted roles for IRX3 in
250 female fertility that include important functions in both ovary and pregnant uterus. In particular,
251 we report that IRX3 functions in early pregnancy to establish successful embryo-uterine
252 interactions. These data provide a foundation for new discoveries of how IRX3 functions in a
253 spatiotemporal manner in the uterus to promote successful embryo-uterine interactions via

254 establishment of proper cell-cell communications to support both decidualization and
255 angiogenesis.

256 Establishment of a robust and healthy vascular network is essential for reproduction as it
257 supports folliculogenesis, ovarian hormone production, ovulation, implantation and embryonic
258 growth [21-23]. Evaluation of the integrity of *Irx3*$^{LacZ/LacZ}$ implantation sites on D7 revealed
259 reduced vascularity with a concomitant decline in the number of implanted embryos, indicating
260 disruptions in reproductive fecundity in *Irx3*$^{LacZ/LacZ}$ mice. Together these data demonstrate that
261 *Irx3* has a role in uterine angiogenesis during embryo implantation.

262 In the murine model, implantation begins late on day D4 when the mouse uterus is
263 receptive to implantation [24]. At D5, the decidualization process begins and the stromal cells of
264 the uterus differentiate into a unique secretory tissue, the decidua. The stromal cells
265 immediately surrounding the embryo are transformed into the primary decidual cells and further
266 expand into the secondary decidual cells until the invasive period is complete [9]. Here, we
267 demonstrate that the expression profile of IRX3 in uterine stromal cells is intimately associated
268 with the decidualization phase of mouse pregnancy. Notably, during the mid-secretory phase of
269 the human menstrual cycle, studies show that *IRX3* expression increases as the uterus
270 becomes receptive to implantation [25-27]. Contrary to mice, the human uterus begins
271 decidualizing in the nonpregnant state, during the mid-secretory phase with an expansion of
272 decidualization once the pregnancy is established [28]. Taken together, these data and our
273 studies have uncovered a conserved physiological timing of *Irx3* expression in the human and
274 murine uterus that corresponds to the onset of decidualization in both species.

275 As decidualization progresses, the uterus undergoes expansive tissue remodeling,
276 critical for proper maternal-fetal interactions. Following the attachment of the blastocyst to the
277 uterine epithelium, the underlying stromal cells differentiate into decidual cells with unique
278 biosynthetic and secretory profiles needed to promote this transformation. We found that IRX3
279 is robustly induced in the decidual tissue during a critical time frame in mouse implantation and

angiogenesis. Factors secreted by the decidualizing stromal cells promote tissue and vascular remodeling, thus, it is conceivable that IRX3, produced by the decidualizing stromal cells, has a role in preparing the uterus for appropriate embryo-uterine interactions. Examination of the decidual program in *Irx3*$^{LacZ/LacZ}$ uteri indicated that initial aspects of the decidualization process are impaired in these mice. It has been suggested that stromal differentiation and angiogenesis are intimately connected processes during pregnancy [15]. Along with a difference in the presence of a subset of decidualization markers, we also observed a substantial decrease in CD31 expression, an endothelial cell marker, in the *Irx3*$^{LacZ/LacZ}$ implantation sites. Collectively, the reduction in vascularization seen at D7 by both histological analysis and immunohistochemistry, demonstrates that ablation of *Irx3* leads to improper vascularization in the mouse uterus during early pregnancy.

Previously, we identified that loss of both *Irx3* and *Irx5* impaired gap junction protein deposition in ovarian follicles, leading to follicle and oocyte death [13]. Here, we discovered a potentially conserved role for *Irx3* in mediating proper cell-cell communication via gap junction expression during embryo implantation. Early studies identified 3 connexins in the human uterus; connexin 26, connexin 32, and connexin 43 [29]. Of these, connexin 43 (GJA1) is the predominant subtype expressed in human and mouse endometrium and localized almost exclusively to the stroma, connecting decidual cells [30]. Conditional knockout of *Gja1* in the mouse uterus resulted in severe subfertility with aberrant differentiation of the uterine stroma and significant reduction in VEGF [15]. Further, maternal decidua isolated from women with recurrent early pregnancy loss was found to have reduced *Gja1* transcripts and protein when compared to controls [31]. The importance of GJA1 regulation during pregnancy is augmented by epidemiological studies that identified taking mefloquine, an anti-malarial compound that blocks GJA1, as a risk factor for spontaneous abortion [32]. Here, our data indicates that IRX3 is instrumental in mediating proper cell-cell communication via GJA1 expression. In the uterus and ovary, GJA1 serves a critical role in establishing communications between cells, promoting

306 both oocyte competence in the ovary and angiogenesis in the uterus during pregnancy [15, 33,
307 34]. Our results indicate that IRX3 promotes successful cell-cell connections allowing for
308 appropriate intercellular cross talk throughout the intimate correspondence of embryo
309 implantation and angiogenesis during pregnancy.

310 Embryo implantation is achieved when a competent oocyte develops into a blastocyst
311 capable of facilitating embryo-uterine interactions with the receptive endometrium. It is clear that
312 IRX3 has a significant role in mouse reproductive health including oocyte competence and
313 endometrial angiogenesis [15, 33, 34]. Impaired uterine receptivity and poor vascularization are
314 major causes of early pregnancy loss. Therefore, understanding how *Irx3* is regulated during
315 this critical window of implantation may provide insights and solutions for female reproductive
316 health and fertility.

**Acknowledgements**

We thank all members of the Jorgensen laboratory for comments and support. We thank Emily Huber and Eowyn Liu for their help with sectioning. We truly appreciate all of the comments, advice, and technical support from the Developmental Endocrinology Group at the University of Wisconsin – Madison School of Veterinary Medicine. We are immensely grateful for Miranda Sun and Daniel Radecki for their support in microscopy trainings and Image J. We would also like to show our gratitude to Annie Novak and Tori Gronemeyer for their exemplary mouse husbandry work.

## Reference List


1. Kim SM, Kim JS. A Review of Mechanisms of Implantation. Dev Reprod 2017; 21:351-359.

2. Psychoyos A. Implantation. In: Greep ROA, E.G.; Geiger, S.R. (ed.) Handbook of Physiology. Washington D.C.: American Physiology Society; 1973: 187-215.

3. Yoshinaga K. Uterine receptivity for blastocyst implantation. Ann N Y Acad Sci 1988; 541:424-431.

4. Parr MBP, E.L. The Implantation Reaction. In: Wynn RMJ, W.P. (ed.) Biology of the Uterus. New York: Plenum Press; 1989: 233-277.

5. Weitlauf HM. Biology of Implantation. In: Knobil EaN, J.D. (ed.) The Physiology of Reproduction. New York: Raven Press Ltd.; 1994: 391-440.

6. Cross JC, Werb Z, Fisher SJ. Implantation and the placenta: key pieces of the development puzzle. Science 1994; 266:1508-1518.

7. Giudice LC, Irwin JC. Roles of the insulinlike growth factor family in nonpregnant human endometrium and at the decidual: trophoblast interface. Semin Reprod Endocrinol 1999; 17:13-21.

8. Carson DD, Bagchi I, Dey SK, Enders AC, Fazleabas AT, Lessey BA, Yoshinaga K. Embryo implantation. Dev Biol 2000; 223:217-237.

9. Ramathal CY, Bagchi IC, Taylor RN, Bagchi MK. Endometrial decidualization: of mice and men. Semin Reprod Med 2010; 28:17-26.

10. Gomez E, Ruiz-Alonso M, Miravet J, Simon C. Human Endometrial Transcriptomics: Implications for Embryonic Implantation. Cold Spring Harb Perspect Med 2015; 5:a022996.

11. Bosse A, Stoykova A, Nieselt-Struwe K, Chowdhury K, Copeland NG, Jenkins NA, Gruss P. Identification of a novel mouse Iroquois homeobox gene, Irx5, and chromosomal localisation of all members of the mouse Iroquois gene family. Dev Dyn 2000; 218:160-174.

12. Peters T, Dildrop R, Ausmeier K, Ruther U. Organization of mouse Iroquois homeobox genes in two clusters suggests a conserved regulation and function in vertebrate development. Genome Res 2000; 10:1453-1462.

13. Fu A, Oberholtzer SM, Bagheri-Fam S, Rastetter RH, Holdreith C, Caceres VL, John SV, Shaw SA, Krentz KJ, Zhang X, Hui CC, Wilhelm D, et al. Dynamic expression patterns of Irx3 and Irx5 during germline nest breakdown and primordial follicle formation promote follicle survival in mouse ovaries. PLoS Genet 2018; 14:e1007488.

14. Zhang SS, Kim KH, Rosen A, Smyth JW, Sakuma R, Delgado-Olguin P, Davis M, Chi NC, Puviindran V, Gaborit N, Sukonnik T, Wylie JN, et al. Iroquois homeobox gene 3

establishes fast conduction in the cardiac His-Purkinje network. Proceedings of the National Academy of Sciences of the United States of America 2011; 108:13576-13581.

15. Laws MJ, Taylor RN, Sidell N, DeMayo FJ, Lydon JP, Gutstein DE, Bagchi MK, Bagchi IC. Gap junction communication between uterine stromal cells plays a critical role in pregnancy-associated neovascularization and embryo survival. Development 2008; 135:2659-2668.

16. Cavodeassi F, Modolell J, Gomez-Skarmeta JL. The Iroquois family of genes: from body building to neural patterning. Development 2001; 128:2847-2855.

17. Gomez-Skarmeta JL, Modolell J. Iroquois genes: genomic organization and function in vertebrate neural development. Curr Opin Genet Dev 2002; 12:403-408.

18. Houweling AC, Dildrop R, Peters T, Mummenhoff J, Moorman AF, Ruther U, Christoffels VM. Gene and cluster-specific expression of the Iroquois family members during mouse development. Mech Dev 2001; 107:169-174.

19. Jorgensen JS, Gao L. Irx3 is differentially up-regulated in female gonads during sex determination. Gene Expr Patterns 2005; 5:756-762.

20. Fu A, Koth ML, Brown RM, Shaw SA, Wang L, Krentz KJ, Zhang X, Hui CC, Jorgensen JS. IRX3 and IRX5 collaborate during ovary development and follicle formation to establish responsive granulosa cells in the adult mouse†. Biol Reprod 2020; 103:620-629.

21. Jiang JY, Macchiarelli G, Tsang BK, Sato E. Capillary angiogenesis and degeneration in bovine ovarian antral follicles. Reproduction 2003; 125:211-223.

22. Yamada OA, M.; Takhana, K.; Iwasa, K.; Hiraga, T.; Hiratsuka, T. Microvasculature of mature bovine follicles and its changes with ovulation. Journal of Reproduction and Development 1994; 40:307-315.

23. Ferrara N, Carver-Moore K, Chen H, Dowd M, Lu L, O'Shea KS, Powell-Braxton L, Hillan KJ, Moore MW. Heterozygous embryonic lethality induced by targeted inactivation of the VEGF gene. Nature 1996; 380:439-442.

24. Paria BC, Huet-Hudson YM, Dey SK. Blastocyst's state of activity determines the "window" of implantation in the receptive mouse uterus. Proc Natl Acad Sci U S A 1993; 90:10159-10162.

25. Tseng LH, Chen I, Chen MY, Yan H, Wang CN, Lee CL. Genome-based expression profiling as a single standardized microarray platform for the diagnosis of endometrial disorder: an array of 126-gene model. Fertil Steril 2010; 94:114-119.

26. Zhang D, Sun C, Ma C, Dai H, Zhang W. Data mining of spatial-temporal expression of genes in the human endometrium during the window of implantation. Reprod Sci 2012; 19:1085-1098.

27. Chan C, Virtanen C, Winegarden NA, Colgan TJ, Brown TJ, Greenblatt EM. Discovery of biomarkers of endometrial receptivity through a minimally invasive approach: a validation study with implications for assisted reproduction. Fertil Steril 2013; 100:810-817.

28. Gellersen B, Brosens IA, Brosens JJ. Decidualization of the human endometrium: mechanisms, functions, and clinical perspectives. Semin Reprod Med 2007; 25:445-453.

29. Jahn E, Classen-Linke I, Kusche M, Beier HM, Traub O, Grummer R, Winterhager E. Expression of gap junction connexins in the human endometrium throughout the menstrual cycle. Hum Reprod 1995; 10:2666-2670.

30. Yu J, Berga SL, Zou W, Yook DG, Pan JC, Andrade AA, Zhao L, Sidell N, Bagchi IC, Bagchi MK, Taylor RN. IL-1beta Inhibits Connexin 43 and Disrupts Decidualization of Human Endometrial Stromal Cells Through ERK1/2 and p38 MAP Kinase. Endocrinology 2017; 158:4270-4285.

31. Nair RR, Jain M, Singh K. Reduced expression of gap junction gene connexin 43 in recurrent early pregnancy loss patients. Placenta 2011; 32:619-621.

32. Nevin RL. Mefloquine blockade of connexin 43 (Cx43) and risk of pregnancy loss. Placenta 2011; 32:712.

33. Ackert CL, Gittens JE, O'Brien MJ, Eppig JJ, Kidder GM. Intercellular communication via connexin43 gap junctions is required for ovarian folliculogenesis in the mouse. Developmental Biology 2001; 233:258-270.

34. Winterhager E, Kidder GM. Gap junction connexins in female reproductive organs: implications for women's reproductive health. Hum Reprod Update 2015; 21:340-352.

## Figure Legends

**Fig 1: *Irx3*$^{LacZ/LacZ}$ causes deficits in uterine vascularization and subfertility.**

(A-D) H&E staining of D7 control (A, C n=6) and *Irx3*$^{LacZ/LacZ}$ (B, D n=6) pregnant uteri. Scale bars, 250μm. The white box in A and B are enlarged in C and D, respectively. A: anti-mesometrial; M: mesometrial; E: embryo. (E, F) Circulating Estrogen (E) and Progesterone (F) were measured at D7 of gestation (WT n=10; *Irx3*$^{LacZ/LacZ}$ n=6). (G) Average number of implantation sites *in utero* at D7 (WT n=8; *Irx3*$^{LacZ/LacZ}$ n=7) and D11 (WT n=3; *Irx3*$^{LacZ/LacZ}$ n=5). Data in G represents the mean ± SEM. Statistics: two-sample t-test, * : $p<0.05$; ** : $p<0.01$.

**Fig 2: *Irx3* expression coincides with embryo implantation.**

(A-F) Immunofluorescence of IRX3 (red) co-labeled with DAPI, a nuclear marker (blue) throughout pregnancy days 4-7 in wild type mice implantation sites (n=3). Scale bars represent 250μm. L: lumen; S: stroma; E: embryo; M: mesometrial**;** A: anti-mesometrial**.** (I) Characterization of *Irx3* transcripts in the WT pregnant mouse uterus at days 4-7 (D4-7). Real time qPCR was determined by setting the expression level of *Irx3* mRNA on D4 of pregnancy to 1.0. Results are reported relative to 36b4 (n=3). Data represent the mean ± SEM of three biological replicates performed in triplicate at each time point.

**Fig 3: Decidualization is impaired in pregnant *Irx3*$^{LacZ/LacZ}$ uteri.**

(A) Real time qPCR was performed using total RNA isolated from implantation sites from pregnant uteri of WT (stippled light gray) and *Irx3*$^{LacZ/LacZ}$ (dark gray) females on day 7 of pregnancy. Data represents the mean ± SEM of three biological replicates performed in triplicate at each time point. Fold change was calculated relative to transcript levels of the WT sample. Statistics: Student's t-test, *$p \leq 0.05$. (B) Immunofluorescence of HAND2, a stromal cell marker (red) co-localized with DAPI, a nuclear marker (blue) at gestation D7 in control (n=4) and *Irx3*$^{LacZ/LacZ}$ (n=3) implantation sites. Scale bars represent 250μm.

**Fig 4: *Irx3*$^{LacZ/LacZ}$ uteri exhibit impaired vascularization by day 7 of gestation.**

(A-F) Immunofluorescence of platelet endothelial cell adhesion molecule (PECAM, CD31, red) co-labeled with DAPI, a nuclear marker (blue) at pregnancy D7 in control (A, C, E, n=3) and *Irx3*$^{LacZ/LacZ}$ (B, D, F, n=3) implantation sites. Scale bars represent 250μm. E: embryo; M: mesometrial**;** A: anti-mesometrial**.** (G) Quantification of relative CD31 fluorescence intensity in the anti-mesometrium (AM) and mesometrium (M). Data represents Mean ± SEM. Statistics: two-sample t-test; **: p<0.01.

**Fig 5: *Irx3*$^{LacZ/LacZ}$ uteri express similar *Gja1* transcripts but abnormal GJA1 protein.**

(A) Real time qPCR results for *Gja1* from pregnant uteri of WT and *Irx3*$^{LacZ/LacZ}$ females on D7 of pregnancy. Data represents the mean ± SEM of three biological replicates performed in triplicate at each time point. Fold change was calculated relative to transcript levels of the WT sample. Statistics: Student's t-test, *p $\leq$ 0.05. (B-I) Immunofluorescence of gap junction protein 1 (connexin 43, GJA1, green) co-labeled with DAPI, a nuclear marker (blue) at gestation D7 in control (B, D, F, H, n=4) and *Irx3*$^{LacZ/LacZ}$ (C, E, G, I, n=5) implantation sites. Images are represented in increasing magnification, scale bars represent 250mm. Arrows highlight single cells that are enlarged within the inset of H and I. (J) Quantification of relative GJA1 fluorescence intensity in the anti-mesometrium (AM, p = 0.01) and mesometrium (M, p = 0.027) in wild type (white bars) vs *Irx3*$^{LacZ/LacZ}$ females (light gray bars). Data represents Mean ± SEM. Statistics: two-sample t-test, *: p<0.05; **: p<0.01.

**Figure 1**

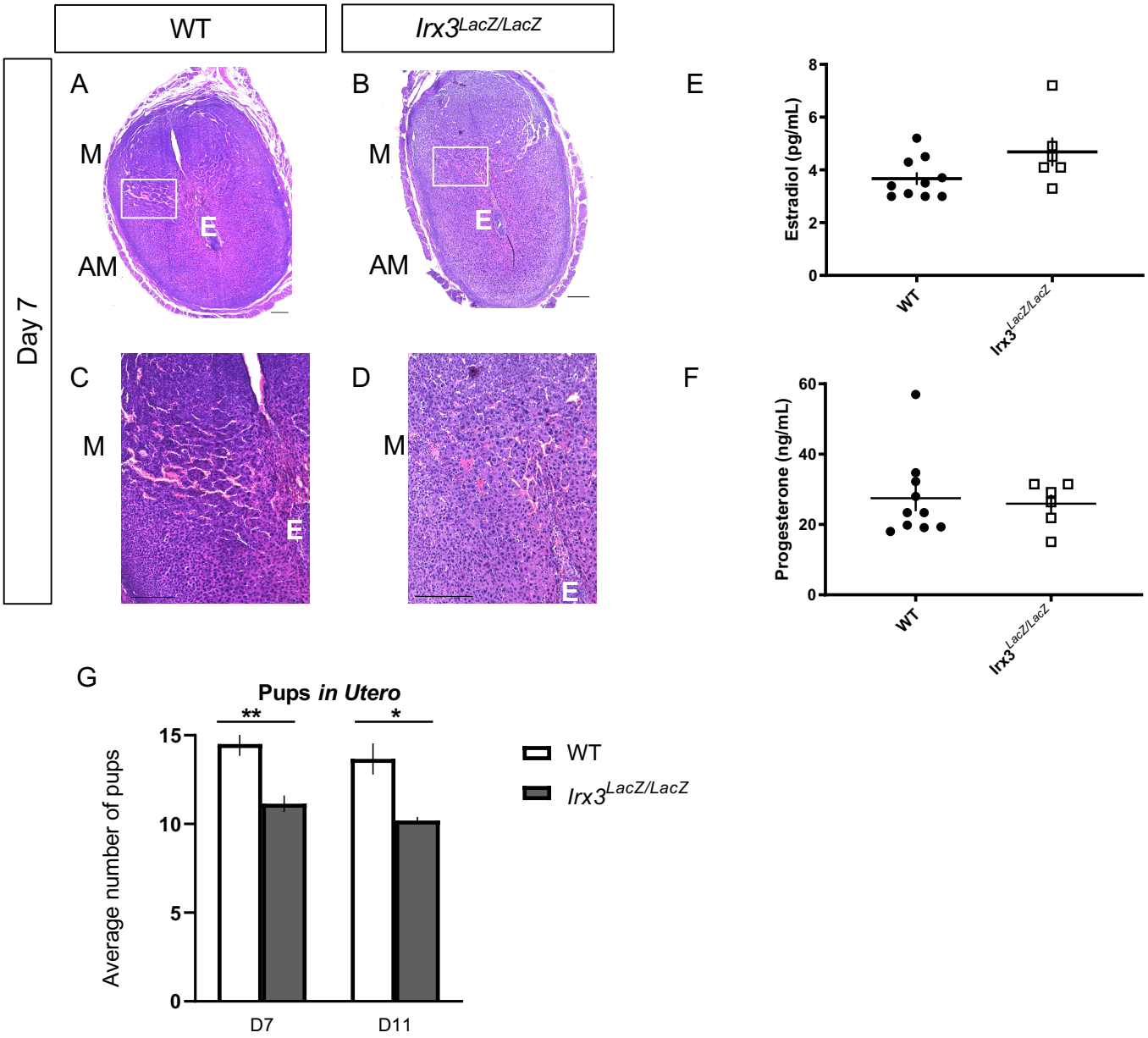


**Fig 1: *Irx3*$^{LacZ/LacZ}$ causes deficits in uterine vascularization and subfertility.**
(A-D) H&E staining of D7 control (A, C n=6) and *Irx3*$^{LacZ/LacZ}$ (B, D n=6) pregnant uteri. Scale bars, 250μm. The white box in A and B are enlarged in C and D, respectively. A: anti-mesometrial; M: mesometrial; E: embryo. (E, F) Circulating Estrogen (E) and Progesterone (F) were measured at D7 of gestation (WT n=10; *Irx3*$^{LacZ/LacZ}$ n=6). (G) Average number of implantation sites *in utero* at D7 (WT n=8; *Irx3*$^{LacZ/LacZ}$ n=7) and D11 (WT n=3; *Irx3*$^{LacZ/LacZ}$ n=5). Data in G represents the mean ± SEM. Statistics: two-sample t-test, * : $p<0.05$; ** : $p<0.01$.

**Figure 2**

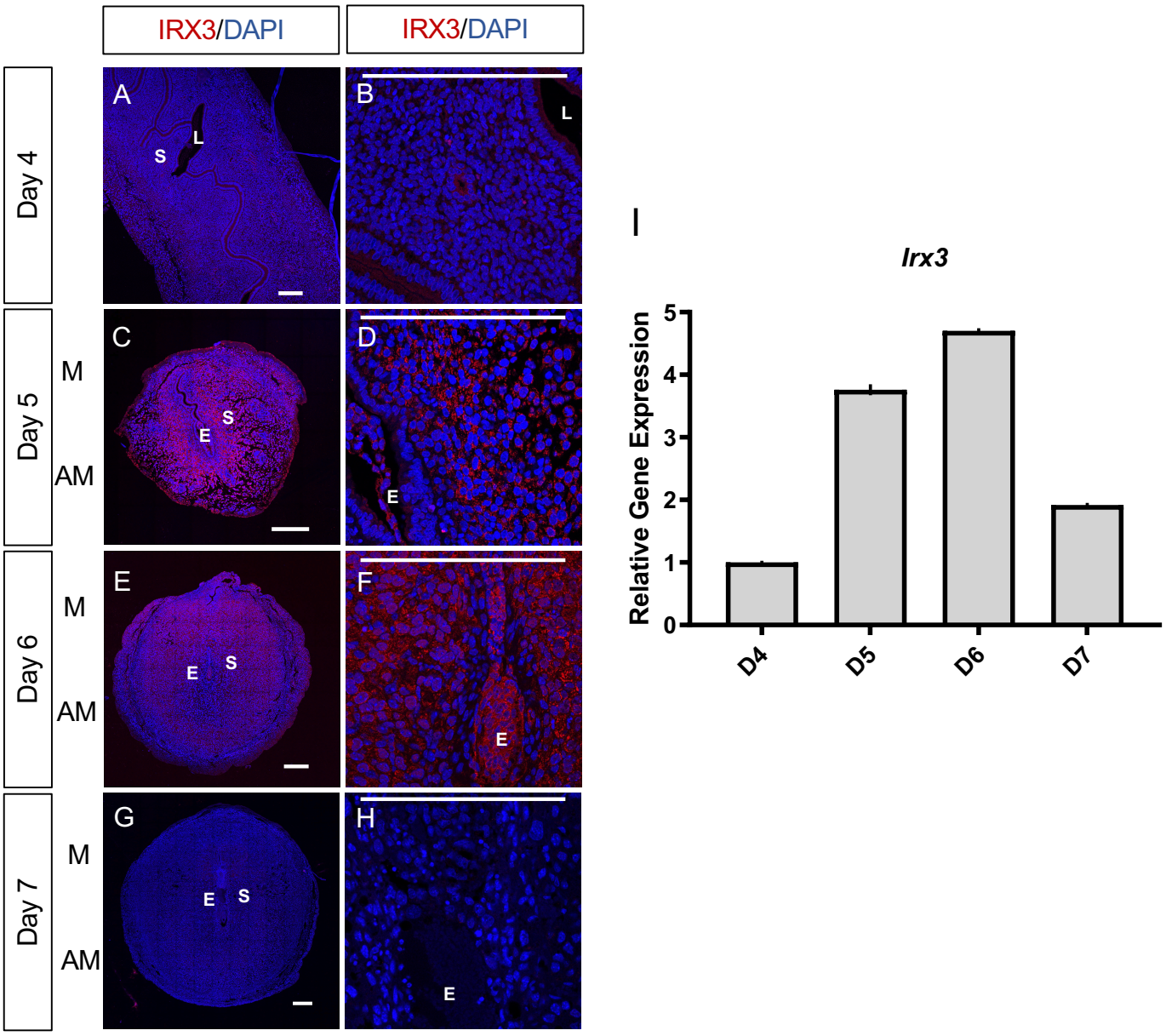


**Fig 2: *Irx3* expression coincides with embryo implantation.**
(A-F) Immunofluorescence of IRX3 (red) co-labeled with DAPI, a nuclear marker (blue) throughout pregnancy days 4-7 in wild type mice implantation sites (n=3). Scale bars represent 250μm. L: lumen; S: stroma; E: embryo; M: mesometrial**;** A: anti-mesometrial**.** (I) Characterization of *Irx3* transcripts in the WT pregnant mouse uterus at days 4-7 (D4-7). Real time qPCR was determined by setting the expression level of *Irx3* mRNA on D4 of pregnancy to 1.0. Results are reported relative to *36b4* (n=3). Data represent the mean ± SEM of three biological replicates performed in triplicate at each time point.

**Figure 3**

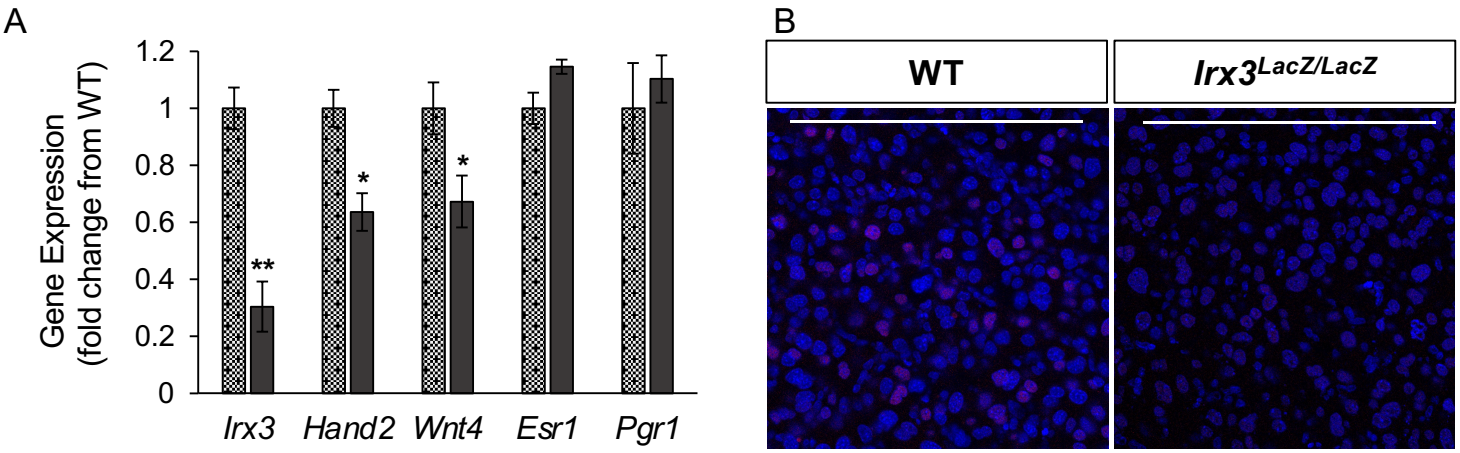


**Fig 3: Decidualization is impaired in pregnant *Irx3*$^{LacZ/LacZ}$ uteri.**
(A) Real time qPCR was performed using total RNA isolated from implantation sites from pregnant uteri of WT (stippled light gray) and *Irx3*$^{LacZ/LacZ}$ (dark gray) females on day 7 of pregnancy. Data represents the mean ± SEM of three biological replicates performed in triplicate at each time point. Fold change was calculated relative to transcript levels of the WT sample. Statistics: Student's t-test, *p $\leq$ 0.05. (B) Immunofluorescence of HAND2, a stromal cell marker (red) co-localized with DAPI, a nuclear marker (blue) at gestation D7 in control (n=4) and *Irx3*$^{LacZ/LacZ}$ (n=3) implantation sites. Scale bars represent 250μm.

**Figure 4**

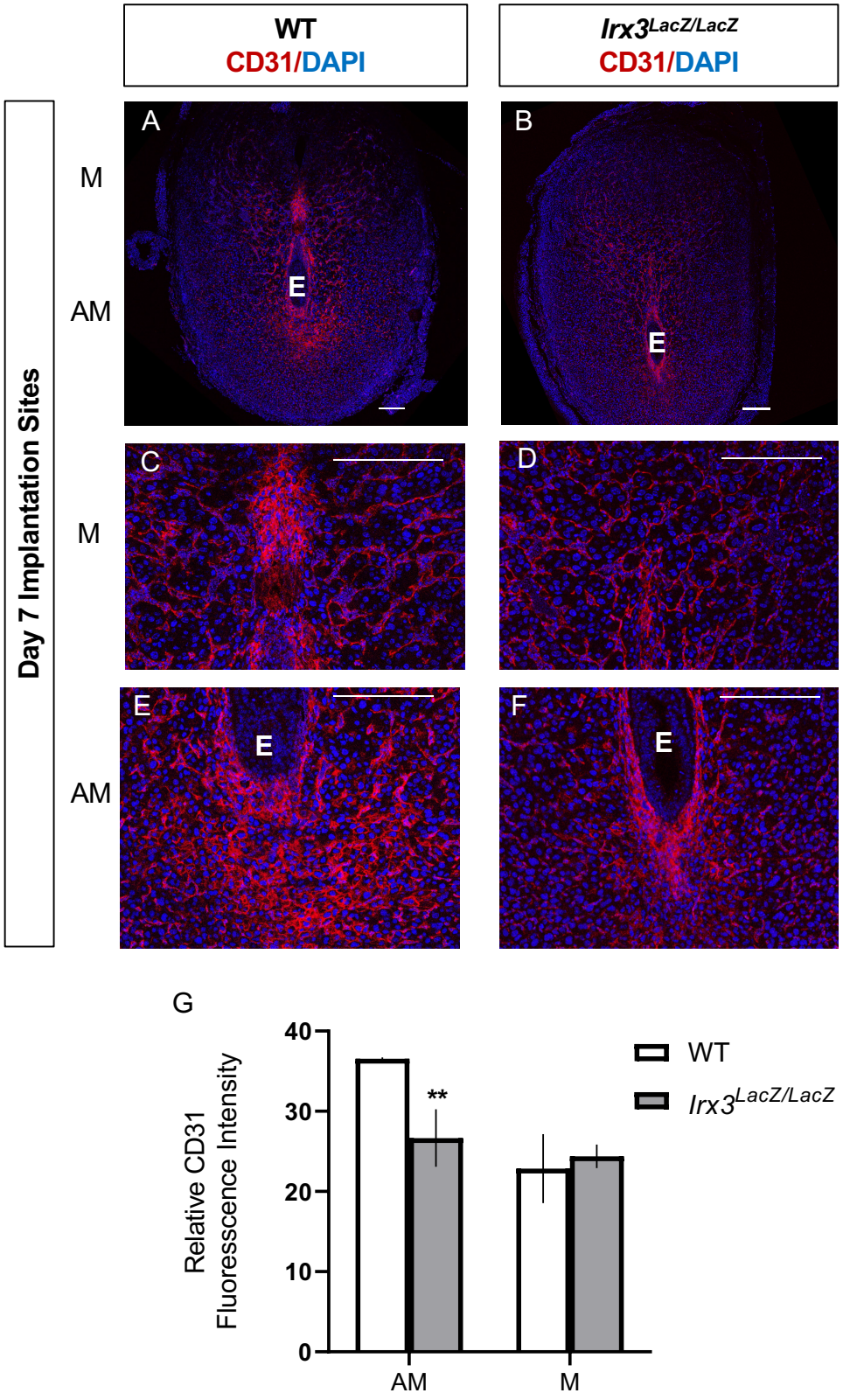


**Fig 4: *Irx3*$^{LacZ/LacZ}$ uteri exhibit impaired vascularization by day 7 of gestation.** (A-F) Immunofluorescence of platelet endothelial cell adhesion molecule (PECAM, CD31, red) co-labeled with DAPI, a nuclear marker (blue) at pregnancy D7 in control (A, C, E, n=3) and *Irx3*$^{LacZ/LacZ}$ (B, D, F, n=3) implantation sites. Scale bars represent 250μm. E: embryo; M: mesometrial**;** A: anti-mesometrial**.** (G) Quantification of relative CD31 fluorescence intensity in the anti-mesometrium (AM) and mesometrium (M). Data represents Mean ± SEM. Statistics: two-sample t-test; ** : $p<0.01$.

**Figure 5**

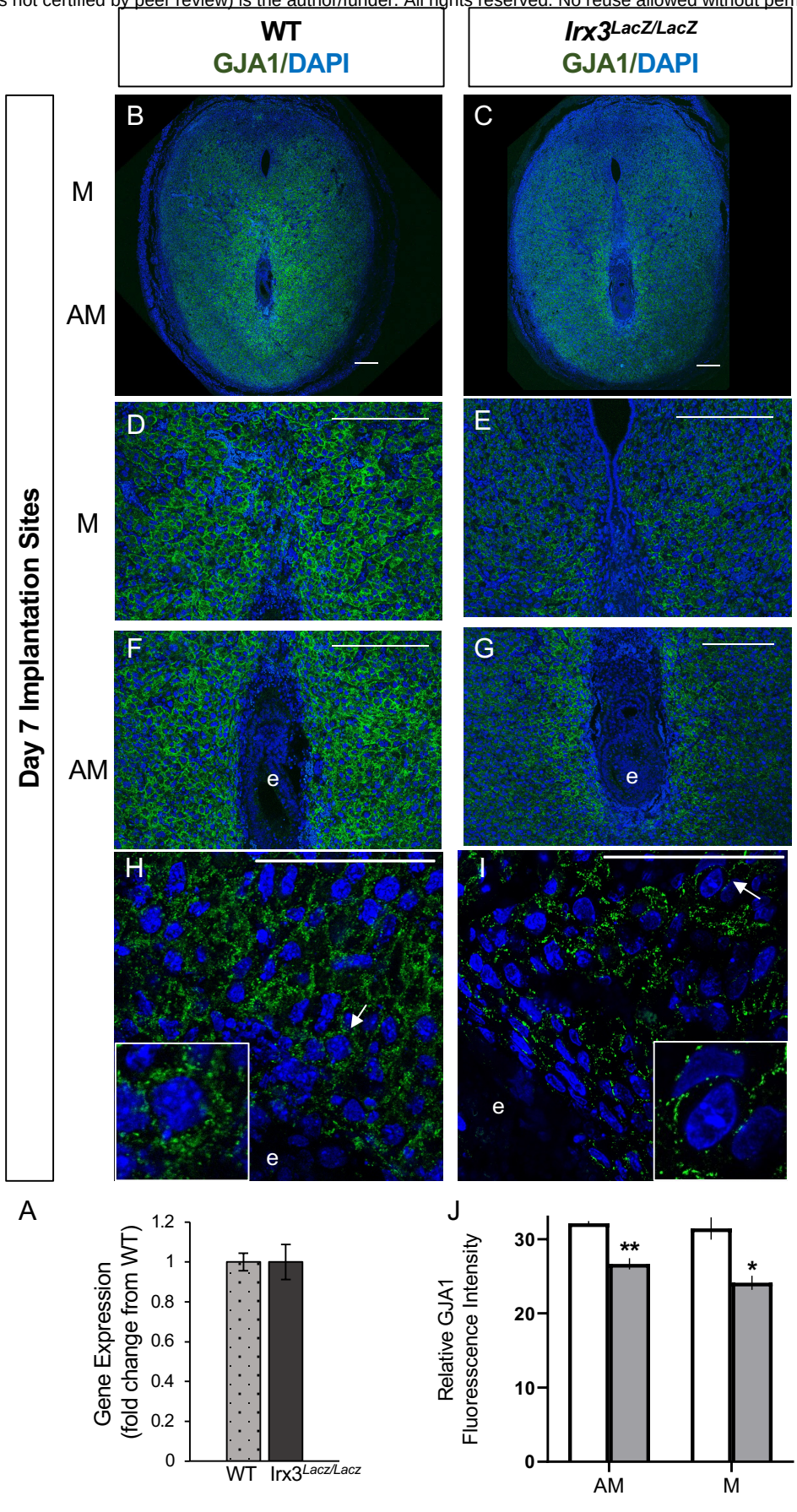

**Fig 5: *Irx3*$^{LacZ/LacZ}$ uteri express similar *Gja1* transcripts but abnormal GJA1 protein.**
(A) Real time qPCR results for *Gja1* from pregnant uteri of WT and *Irx3*$^{LacZ/LacZ}$ females on D7 of pregnancy. Data represents the mean ± SEM of three biological replicates performed in triplicate at each time point. Fold change was calculated relative to transcript levels of the WT sample. Statistics: Student's t-test, *$p \leq 0.05$. (B-I) Immunofluorescence of gap junction protein 1 (connexin 43, GJA1, green) co-labeled with DAPI, a nuclear marker (blue) at gestation D7 in control (B, D, F, H, n=4) and *Irx3*$^{LacZ/LacZ}$ (C, E, G, I, n=5) implantation sites. Images are represented in increasing magnification, scale bars represent 250μm. Arrows highlight single cells that are enlarged within the inset of H and I. (J) Quantification of relative GJA1 fluorescence intensity in the anti-mesometrium (AM, $p = 0.01$) and mesometrium (M, $p = 0.027$) in wild type (white bars) vs *Irx3*$^{LacZ/LacZ}$ females (light gray bars). Data represents Mean ± SEM. Statistics: two-sample t-test, *: $p<0.05$; **: $p<0.01$.

# Supplementary Table 1

**Supplementary Table S1:** Antibody Information

| Antibody | Dilution | Company | Catalogue number | Antigen Retrival |
|---|---|---|---|---|
| IRX3 | 1:100 | Invitrogen | PA5-35149 | EDTA |
| HAND2 | 1:50 | Abcam | ab200040 | Citrate |
| FRA1 | 1:100 | Invitrogen | PA5-76185 | Citrate |
| CD31 | 1:200 | Abcam | ab182981 | EDTA |
| GJA1 | 1:250 | Abcam | ab11370 | Citrate |